Materials & Design 131 (2017) 144–155

Contents lists available at ScienceDirect

Materials & Design

journal homepage: www.elsevier.com/locate/matdes

Titanium/nanodiamond nanocomposites: Effect of nanodiamond on microstructure and mechanical properties of titanium

Faming Zhang[a,*], Suli Liu[a], Peipei Zhao[a], Tengfei Liu[a], Jing Sun[b]

[a] Jiangsu Key Laboratory for Advanced Metallic Materials, School of Materials Science and Engineering, Southeast University, 211189 Nanjing, China
[b] State Key Laboratory of High Performance Ceramics and Superfine Microstructure, Shanghai Institute of Ceramics, Chinese Academy of Sciences, 200050 Shanghai, China

ARTICLE INFO

Keywords:
Metal-matrix composites (MMCs)
Nanoparticles
Mechanical properties

ABSTRACT

Titanium (Ti)/nanodiamond (ND) nanocomposites with potential for biomedical applications were prepared by using spark plasma sintering technique. By means of X-ray diffraction, scanning electron microscopy, transmission electron microscopy and mechanical analysis, the Ti/ND nanocomposites were investigated, and thus the effect of ND on the microstructural and mechanical properties of Ti matrix was demonstrated. Experimental results showed that the Ti/ND nanocomposites exhibited pure α-Ti phase with ND concentrations from 0.1 to 0.35 wt% and with in-situ formed nano-TiC phase in 0.5–2.0 wt% NDs. The nanoindentation hardness, Young's modulus and compressive yield strength of the Ti/ND nanocomposites were significantly improved, as ND was incorporated into the Ti matrix. Improvements of hardness (60.2%), Young's modulus (27.4%) and compressive yield strength (24%) were achieved by doping of 0.5 wt% NDs in the Ti matrix but at an expense of ductility. The Ti/0.35 wt% NDs nanocomposites have the best integrated mechanical properties. These improvements could be ascribed to the outstanding mechanical properties of ND, homogeneous dispersion of ND nanoclusters, Orowan strengthening with ND/nano-TiC and carbon atom solid solution strengthening in the Ti/ND nanocomposites.

GRAPHICAL ABSTRACT

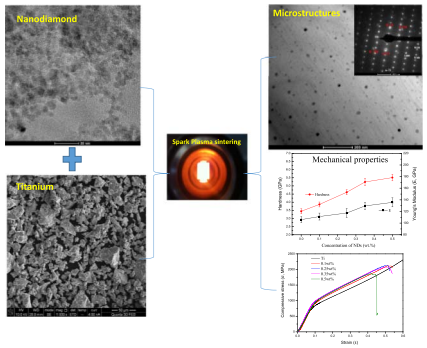

1. Introduction

Titanium (Ti) has found extensively applications in many engineering industries such as aerospace, chemical and biomedical fields due to their light weight, high specific strength, excellent chemical resistance and biocompatibility [1,2]. Pure Ti was once used as biomaterials, but the disadvantage for the use of pure Ti as implant materials is its low strength and insufficient hardness, which limit its application in artificial implants of hip and knee prostheses [3,4]. Ti alloys containing elements of vanadium (V), aluminum (Al), iron (Fe),

* Corresponding author.
E-mail address: fmzhang@seu.edu.cn (F. Zhang).

http://dx.doi.org/10.1016/j.matdes.2017.06.015
Received 24 February 2017; Received in revised form 4 June 2017; Accepted 6 June 2017
Available online 07 June 2017

niobium (Nb), zirconium (Zr), tantalum (Ta), molybdenum (Mo), nickel (Ni), gold (Au), silicon (Si), manganese (Mn) and so forth have been investigated for biomedical applications [5–14]. The mechanical properties of the Ti metal have been greatly enhanced by the alloying method. However one main problem for the Ti alloys is that metal ion release may induce cytotoxicity and damage human body [15,16].

Alternatively, Ti metal matrix composites (MMCs) with nanostructured reinforcement can offer superior mechanical properties and reduced weight. Carbon nanotubes (CNTs) and graphene make contributions to the development of new materials with outstanding mechanical properties because of its exceptional mechanical and high aspect ratio [17–19]. Many literatures showed significant achievements in Ti MMCs reinforced with carbon nanotubes (CNTs) and graphene [17–23]. However, the CNTs and graphene are both cytotoxic, which limit their applications in biomedical field [24–28]. Shvedova et al. [25] reported that exposure of human epidermal keratinocytes to CNTs produced oxidative stress and cellular toxicity, in addition it resulted in ultrastructural and morphological changes in cultured human cells. Graphene leads to significant interactions with membrane lipids leading to direct physical toxicity or adsorption of biological molecules leading to indirect toxicity, and it has a potential to induce foreign body tumors [26–28]. Another promising nanocarbon material, nanodiamonds (NDs) have excellent mechanical properties, high surface areas and tunable surface structures [29]. Especially, NDs are non-toxic and biocompatible comparing to CNTs and graphene, which make them very promising for biomedical application [30]. Diamond and diamond-like carbon films have been used for robust implant coatings [31,32] and NDs have been applied as stable cellular biomarkers [33], probe for biolabeling, and foundation for chemotherapeutic drug carriers and anti-inflammatory interfaces [34] as well as for localized cancer treatment [35]. By adding NDs into polymer, Cu and Al matrix, superior wear resistance, hardness and excellent bending strength can be obtained, which are much higher than that with CNTs [36–40]. Furthermore, owing to higher mechanical strength of NDs, the final particle size of 4–5 nm can be preserved without damaging its structures during milling process. To the best of our knowledge, there is just few work focusing on Ti MMCs reinforced with NDs. Melendez et al. [41] have reported that the bending strength of Ti MMCs reinforced with NDs (1.8% vol.) was higher than that with the same amount of CNTs, which were fabricated via normal powder metallurgy method. However, the optimal amount of NDs, the quantitative evaluation of mechanical properties and the strengthening mechanism of Ti MMCs reinforced with NDs have never been reported.

The purpose of this work is to study the preparation, effect of the ND on the microstructures and mechanical properties of the Ti matrix. The Ti/ND nanocomposites were prepared by spark plasma sintering (SPS) technique which can enable MMCs with favorable properties to be consolidated by shorter holding times and relatively lower temperatures [42–45]. The effects of ND amounts on the microstructure and mechanical properties of Ti MMCs are investigated. Additionally, the strengthening mechanisms of NDs in the Ti MMCs are explored. The possible biomedical applications of the Ti/ND nanocomposites is discussed.

2. Experimental procedure

2.1. Materials

Ti powders were prepared by hydride-dehydride method with purity of 99.5% and mean particle size of 10–44 μm (Nanjing Mingshan Advanced Materials Co. Ltd., China). Spherical NDs were fabricated by detonation technique and used as reinforcements with purity of > 98%, 5 nm in diameter and mean specific surface area of 350 m^2/g (Tianjin Qianyu Superhard Materials Co. Ltd. China).

2.2. Nanocomposite fabrication

NDs were mixed with Ti powders with various fractions of 0.1, 0.25, 0.35, 0.5 wt% and up to 2.0 wt%. They were mixed through a two-stage process. The schematic illustration of fabrication process of the Ti MMCs reinforced with NDs is presented in Fig. 1. In stage I, the NDs were dispersed in ethanol solution using ultrasonication for 30 min. The Ti powders were dispersed in another glass cup in the same way. Afterwards the two kinds of powder solutions were mixed together and stirred using ultrasonication for 30 min. In addition, they were mixed by using a high energy planetary ball milling machine (QM-3SP2) with ball to powder ratio of 10:1 for 5 h at 250 RPM. The powder mixtures were dried in a vacuum oven, loaded into a cylindrical graphite die (Φ10 mm) and consolidated using spark plasma sintering (SPS) in stage II. The SPS experiments were conducted in a spark plasma sintering system (FCT-HP-D5, FCT Systeme GmbH, Germany) installed at Southeast University. The sintering temperature was measured by a

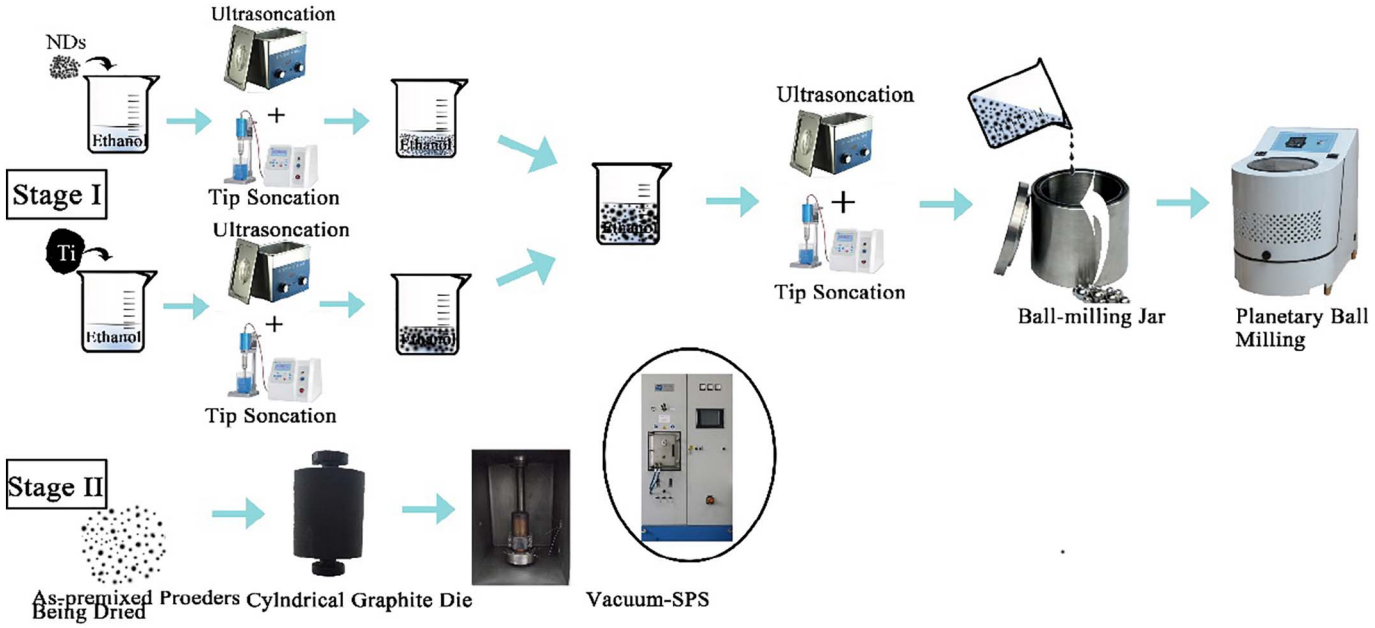

Fig. 1. Schematic illustration of processing procedure for the Ti/NDs nanocomposites.

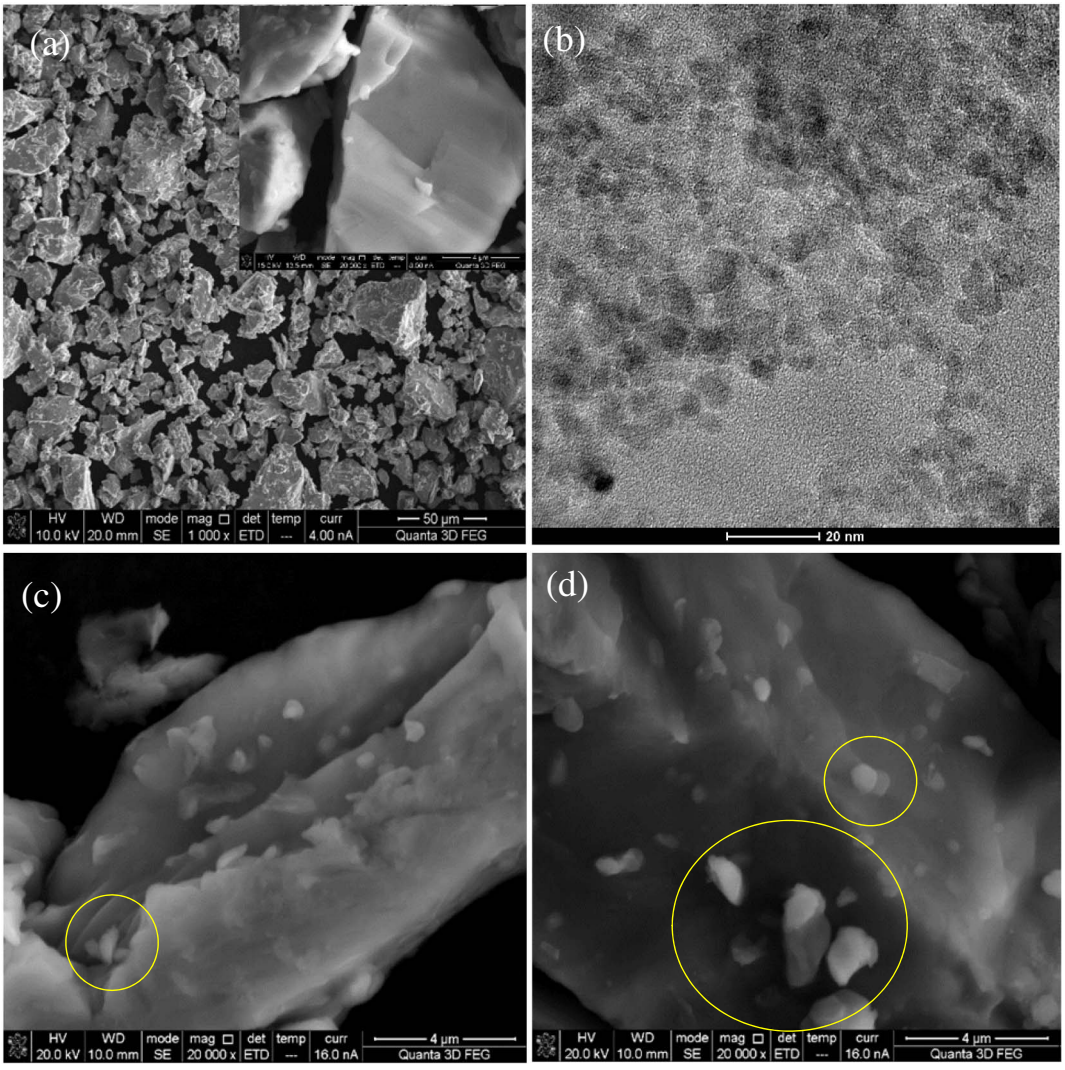

Fig. 2. SEM micrographs of pure Ti powders with inserted high magnification image (a), TEM micrograph of NDs (b), SEM micrographs of the powder mixtures of Ti/0.25% NDs (c) and Ti/0.5%NDs (d).

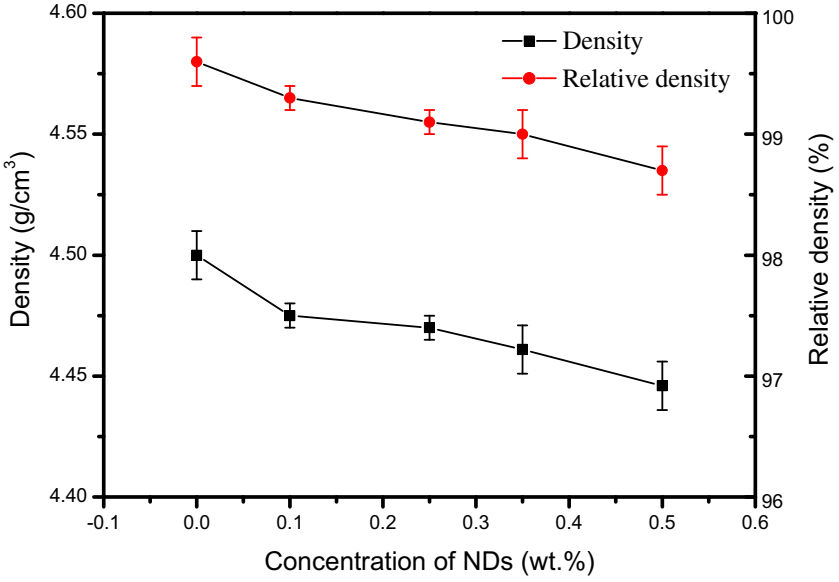

Fig. 3. Density and relative density of the Ti/NDs nanocomposites as a function of concentration of NDs.

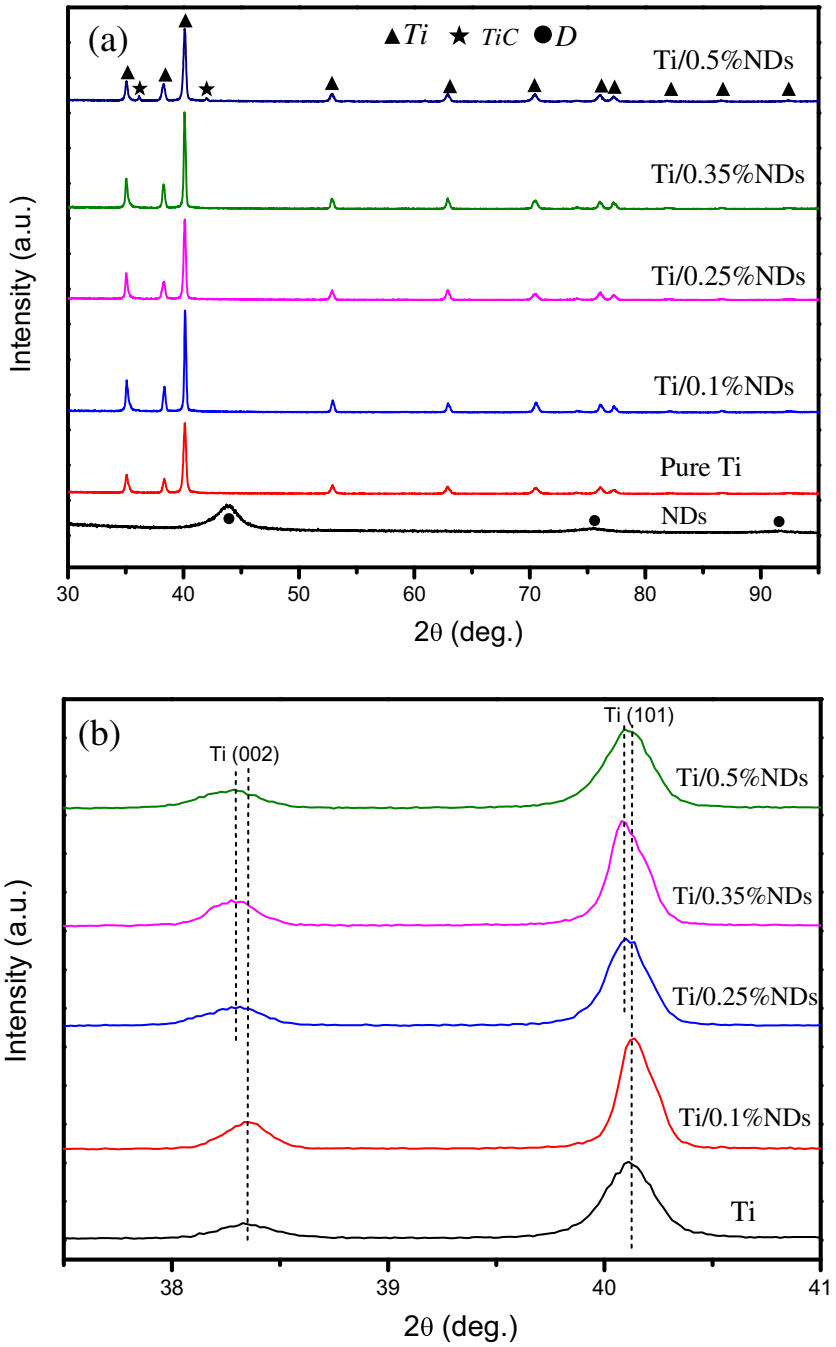

Fig. 4. XRD patterns of the pure Ti and Ti/NDs nanocomposites fabricated via SPS (a) and the enlarged area (2θ 37°–41°) of the XRD pattern (b).

thermocouple (TC). The sintering parameter was set as 900 °C for 10 min at a pressure of 60 MPa in vacuum with a heating rate of 100 °C/min. The resulting sintered specimen have diameters of 10.0 mm and heights of 12.0 mm.

2.3. Characterization techniques

The relative densities of all the sintered Ti MMC samples were determined using Archimedes principle in water at room temperature. The phase compositions of the samples were identified by X-ray diffraction system (XRD, D8 discovery, Bruker) with Cukα monochromatic radiation. The microstructures of these sintered samples were characterized using optical microscopy (OM, Olympus, BX60M), field-emission scanning electronic microscopy (FESEM, Sirion, FEI) equipped with energy-dispersive X-ray spectrometer (EDS), and transmission electron microscopy (TEM, Tecnai, FEI) with selected area electron diffractions (SAD). The hardness and Young's modulus of the samples were measured by a nanoindentation test system (Micro Materials-NanoTest). A calibrated diamond Berkovich indenter tip was used for indentation at the maximum load of 5 mN and loading-unloading rate of 0.25 mN/s. Compression tests were conducted on a universal testing machine (CMT5305, MTS) with a strain rate of 0.5 mm/min. Five samples of each group was used for statistical analysis of the mechanical properties.

3. Results and discussions

3.1. Powder morphology

Fig. 2(a) shows the SEM micrograph of pure Ti powders. The raw Ti

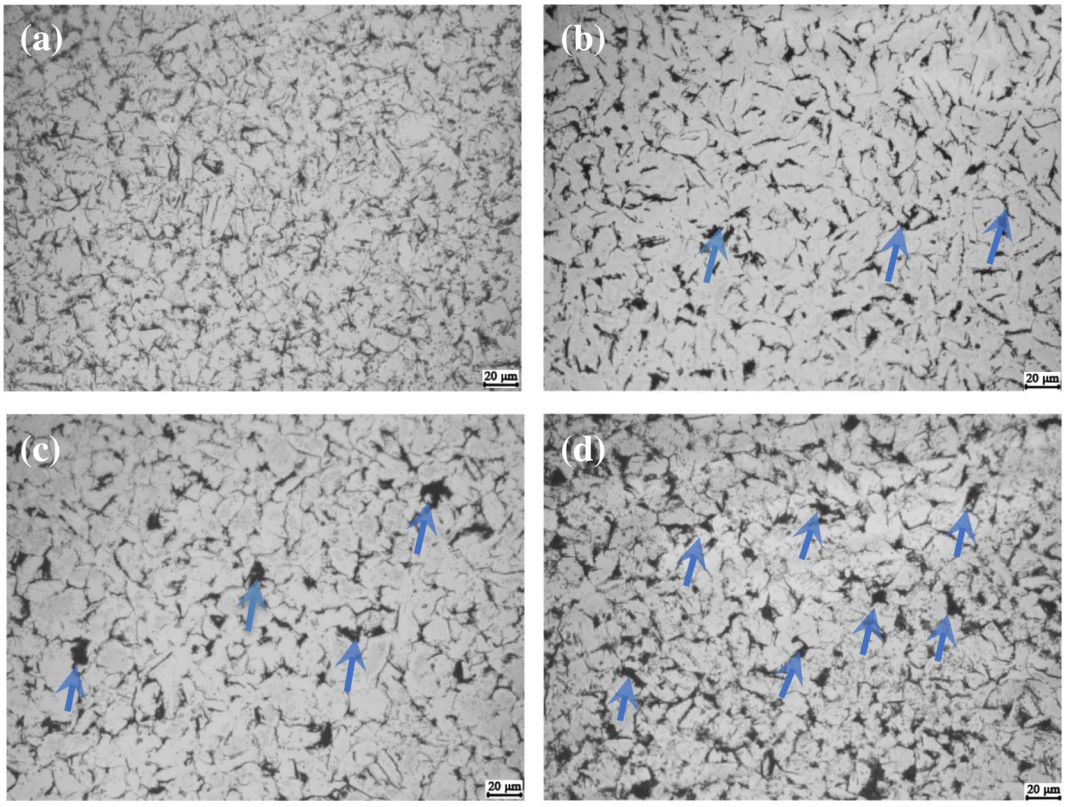

Fig. 5. Metallographic micrographs of Ti (a) and Ti/NDs nanocomposites fabricated by SPS containing various ND concentrations: 0.1% (b), 0.25% (c) and 0.5% (d).

powders exhibit irregular shape with particle sizes of 10–44 μm. The TEM image of NDs is shown in Fig. 2(b). The round nanometer sized particles can be easily recognized in the image with a uniform particle size distribution about 5 nm. Fig. 2 (c, d) exhibits the SEM micrographs of morphologies of the powder mixtures of Ti/0.25%NDs and Ti/0.5% NDs after mixing using the state I process in Fig. 1. The nearly spherical NDs particles are uniformly dispersed in the Ti matrix. There are more ND particles on the surface of Ti powders in the sample of Ti/0.5%NDs (Fig. 2d). As can be seen from the micrographs, there are a little agglomerations in the ND powder particles as noted by circles. It can be due to the nanometered particle size, large specific surface area and high surface energy of the NDs leading to this agglomeration [46]. Relatively uniform Ti/NDs mixture powders were prepared by using the mixing process in Fig. 1.

3.2. Densities of the nanocomposites

The powder mixtures were consolidated by the SPS technique as shown in Fig. 1 (Stage II). Fig. 3 shows the densities and relative densities of the Ti/NDs nanocomposites as a function of ND concentrations. The values in Fig. 3 show that the relative densities of the Ti/NDs nanocomposites are all exceeding 98% (mean Arch. Density 4.42 g/cm^3), and two groups' nanocomposites (0.1% and 0.25%) present values up to 99.5%. It reveals that the dense Ti/NDs nanocomposites can be fabricated via the SPS process at a relatively low temperature (900 °C). Actually, various temperatures were tried at 850, 900, 950 and 1000 °C for the SPS of the Ti/NDs nanocomposites. However their relative densities didn't increase at the temperatures higher than 900 °C. In addition, it is observed that the relative densities of the nanocomposites relating to pure Ti decreased with an increase of the weight fraction of NDs (in the range of 0.1–0.5%). The more amount of NDs are added, the less densification is obtained. However, the variations of relative densities among these specimens are very small (< 0.2%), which suggests that the content of NDs only has small impact on the density of the Ti MMCs reinforced with NDs.

3.3. Phases of the nanocomposites

Fig. 4 shows XRD patterns of the pure Ti, NDs and the Ti/NDs nanocomposites containing 0.1, 0.25, 0.35 and 0.5% NDs. As can be seen, both of Ti and TiC peaks can be observed in the XRD patterns of the Ti MMCs with 0.5% NDs. The presence of nano-TiC phase in the 0.5% ND composite is confirmed by the broad and weak peaks at 2θ values of 36.15° and 42.02°, which are indexed as TiC (111) and (200), respectively. The formation of nano-TiC is due to the reaction between Ti and NDs in the Ti/0.5% ND composites during the SPS processing at 900 °C, which is a spontaneous reaction. The nano-TiC phases are also existed in the nanocomposites with 0.75, 1.0, 1.5 and 2.0 wt% NDs, which are similar to the 0.5%ND composites (Fig. S1). However, only Ti peaks without any nano-TiC peak are found in the other Ti MMCs samples (0.1–0.35%). The reason may be due to the amount of NDs is so small and the minimal nano-TiC phase cannot be detected by the XRD [47]. Fig. 4(b) exhibits the enlarged two main Ti peaks of (101) and (002) according to Fig. 4(a). As shown, the Ti main peaks have shifted to smaller 2θ angle slightly. It means that there is tensile residual strength in the nanocomposites, which is because of the dissolution of carbon atoms into the hcp structured lattice of α-Ti. However, the shifting stops when NDs content is over 0.25% in the nanocomposites. The limit of carbon solubility in the α-Ti substrate is about 0.05% at room temperature, which retarded the distortion of lattice [48–49].

3.4. Surface microstructures of the nanocomposites

Fig. 5 shows the metallographic optical images of the pure Ti and Ti/NDs nanocomposites synthesized by the SPS process. It is found that all specimens consist of near equiaxial a-Ti phase as matrix, and there are some dark voids (marked with arrows) distributed in the matrix of nanocomposites. Some differences among these images can be

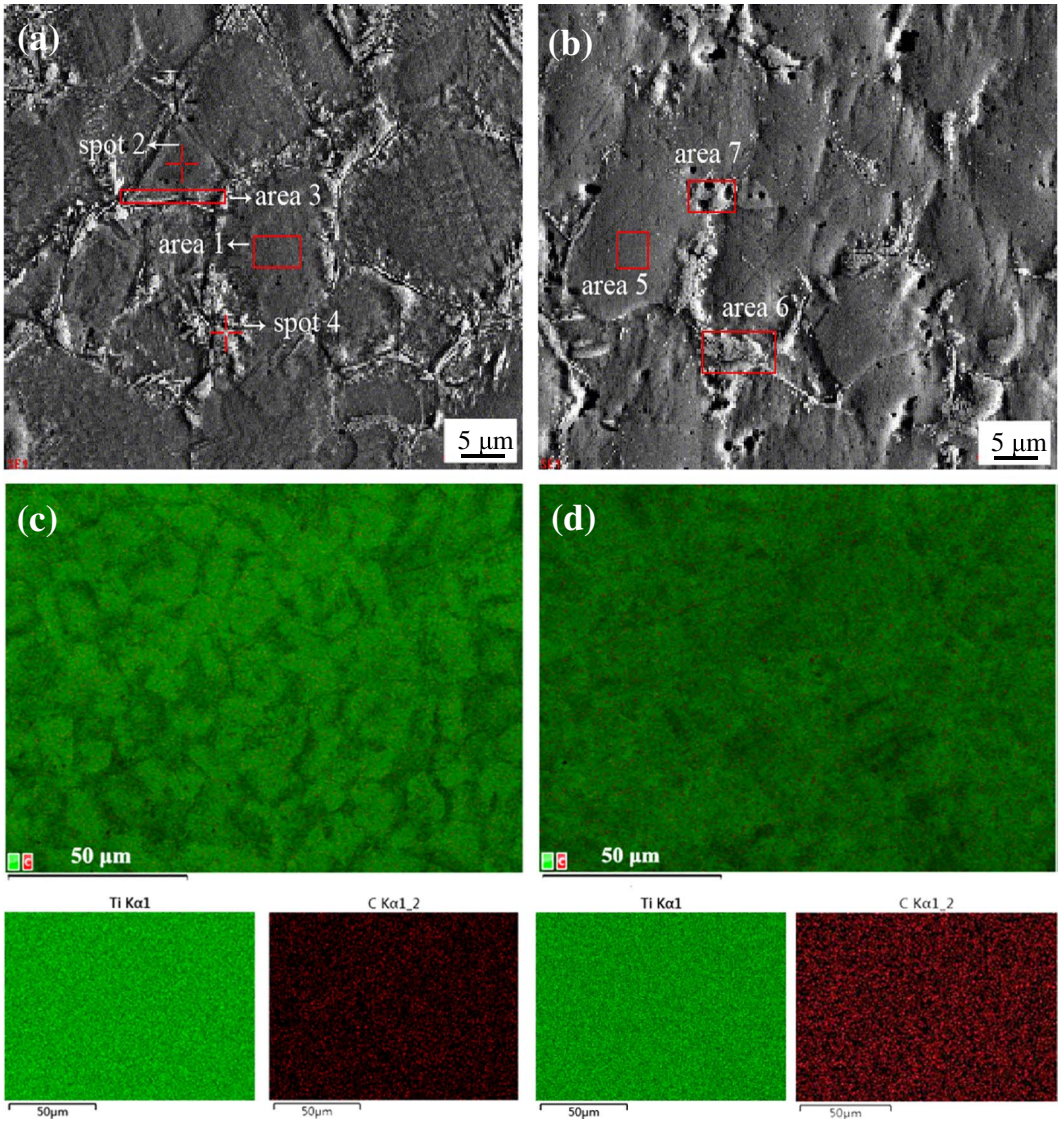

Fig. 6. SEM micrographs of the Ti/NDs nanocomposites of Ti/0.25% NDs (a) and Ti/0.5% NDs (b) with EDS inspection spots and areas imprinted; EDS elemental maps of Ti/0.25% NDs (c) and Ti/0.5% NDs (d) exhibiting the distribution of Ti and C elements.

Table 1
EDS results of marked spots and areas on grain (G) and grain boundary (GB) in the Ti/NDs nanocomposites as shown in the Fig. 6(a, b).

Samples	Area (or spot)	Ti (mass%)	C (mass%)	Ti (at%)	C (at%)
Ti/0.25 wt% NDs	1 G	97.50	2.50	90.74	09.26
Ti/0.25 wt% NDs	2 G	96.88	3.12	88.62	11.38
Ti/0.25 wt% NDs	3 GB	97.28	2.72	89.98	10.02
Ti/0.25 wt% NDs	4 GB	96.66	3.34	87.89	12.11
Ti/0.5 wt% NDs	5 G	93.93	6.07	79.51	20.49
Ti/0.5 wt% NDs	6 GB	93.74	6.26	78.96	21.04
Ti/0.5 wt% NDs	7 GB	92.62	7.38	75.88	24.12

observed. The amounts of the voids increased with the fraction of NDs increases from 0.1 to 0.5%. It is due to the increased amount of ND additives reduced the relative densities of the composites. In addition, the grain boundaries become clearer and grain sizes become smaller. It is because the dispersoids of NDs and the in-situ formed nano-TiC existing in the metal matrix can pin and hinder migration of the Ti grain boundaries.

Fig. 6 shows the SEM micrographs of the etched surfaces of Ti/0.25% NDs and Ti/0.5% NDs nanocomposites. The grain sizes are about 20–30 μm with clear grain boundaries (Fig. 6a, b). It can be observed some bright small particles on the grain surfaces and grain boundaries. Furthermore, few micropores are found on the grain boundaries of the Ti/0.5% NDs composites. It is confirmed that the relative density of the Ti/0.5%NDs composite is less than the Ti/0.25%NDs. EDX analysis is carried out to examine the dispersion of NDs. Fig. 6 (c, d) exhibits EDX maps of the Ti/0.25%NDs and Ti/0.5%NDs nanocomposites indicating the distributions of C and Ti elements. It can be seen that there are much higher C concentrations in the Ti/0.5% NDs sample because of the increased amount of NDs. These two images display that the distributions of C elements are both in the grain boundaries and inside of the grains. In order to determine the concentration locations of the NDs, EDX spot and area inspections are performed, as marked in the SEM images of Fig. 6 (a, b). Table 1 summarized the EDX results of the Ti and C percentages in the nanocomposites. It is found that the C concentration has a slightly increase (0.5–0.8 at% higher) in grain boundaries compared with inside of grains in both of the two nanocomposites. The fact indicates the NDs are easier to concentrate in the grain boundaries than in the grains. In Table 1, the value of carbon reaches the highest level for Area 7 when compared to other areas and spots, this area is the region that has the most micropores as seen in Fig. 6(b). For choosing an area that has a lot of micropores for EDS analysis is to prove that the NDs gathering resulted in decreases in

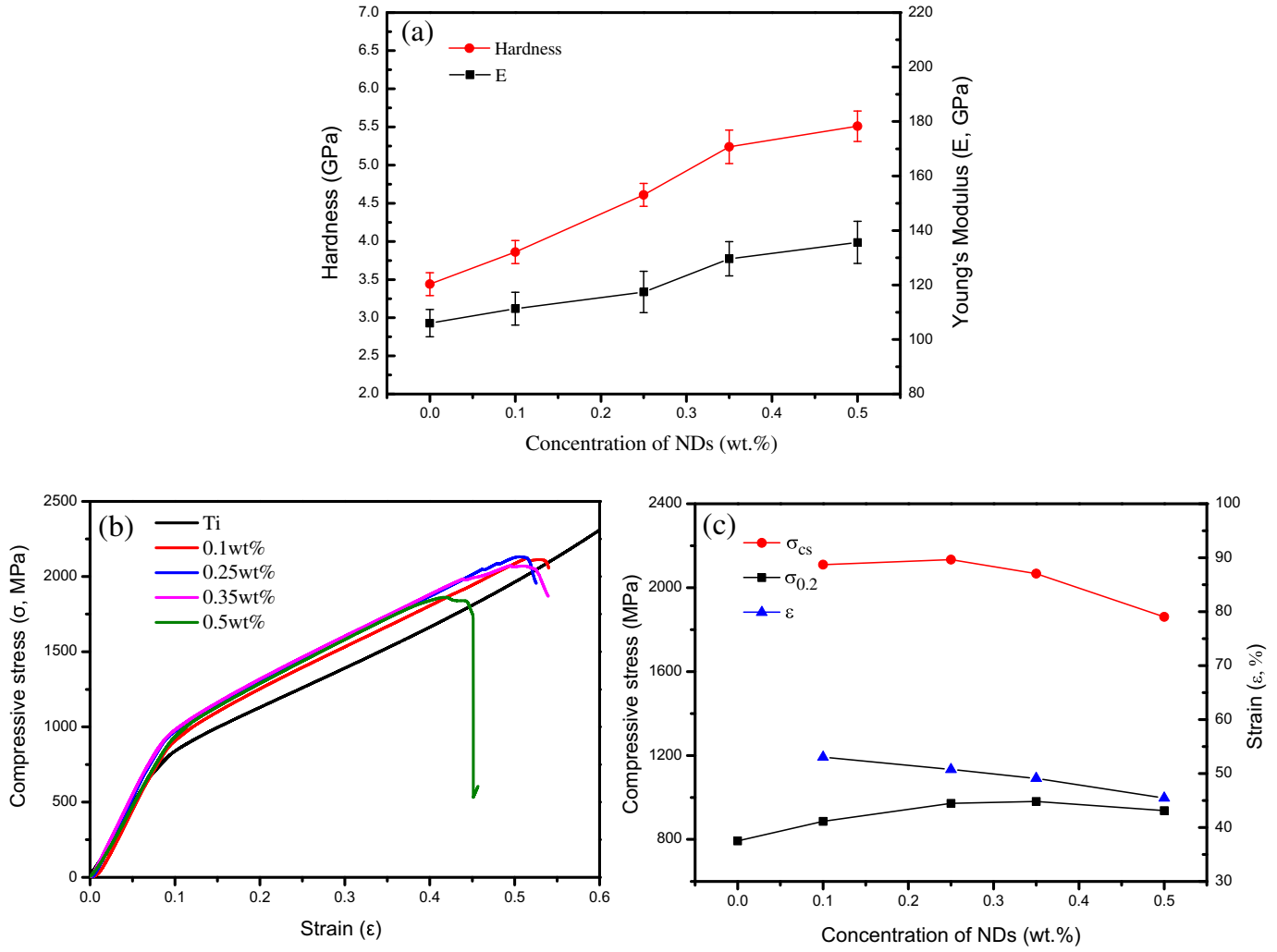

Fig. 7. Mechanical properties of the Ti and Ti/NDs nanocomposites: Nanoindentation Hardness and Young's modulus (a), compressive stress-strain curves (b), compressive stress and strain of the Ti/NDs as a function of ND concentrations (c).

relative density of the nanocomposites.

3.5. Mechanical properties of the nanocomposites

Fig. 7(a) presents the nanoindentation hardness (H) and Young's modulus (E) of pure Ti and Ti/NDs nanocomposites. It can be seen that the hardness of the nanocomposites is remarkably increased with the concentration of the NDs increases. When the weight fraction of NDs increases from 0 to 0.5%, the hardness of the nanocomposite has a sharp growth and then goes steady. The Ti/0.5%NDs samples have the maximum hardness value of 5.51 ± 0.20 GPa. It shows 60.2% increment in hardness compared with the pure Ti (3.44 ± 0.15 GPa) that sintered under the same condition. This indicates that a small amount of NDs has great effect on the hardness improvement of the nanocomposites. In addition, the hardness of Ti/0.35% NDs composite is 5.24 ± 0.22 GPa and is just 3.1% lower than that of the Ti/0.5%NDs composite. An increase in hardness leads to an improvement in wear and scratch resistance of Ti matrix. It can contribute to promote the application of Ti composites in orthopedic implants [50]. The Young's modulus obtained by the nanoindentation exhibits an increasing trend with the ND amounts from 0 to 0.5%. The Young's modulus is increased from mean value of 106 GPa (Ti) to 111 GPa (Ti/0.1%NDs), 117 GPa (Ti/0.25%NDs) and 129 GPa (Ti/0.35%NDs), respectively. The Ti/0.5%NDs composites exhibit the highest E value of 135 GPa.

Room temperature compressive tests were carried out to assess the stress-strain curves for the Ti/NDs nanocomposites (Fig. 7b). The Ti/NDs nanocomposites all exhibit much higher yield strength (0.2% off-set, $\sigma_{0.2}$) when compared to that of pure Ti. However the ductility of the Ti/0.5%NDs has remarkably reduced to 0.45 (45%). Fig. S2 demonstrates the compressive stress-strain curves of the Ti composites with higher ND amounts of 0.75, 1.0, 1.5 and 2.0 wt%. However, the ductility of the nanocomposites decreased too much from 0.41 to 0.34. It makes the Ti composites too brittle to be used in industry. It indicates that the NDs doping amount should be lower than 0.35 wt% for the Ti MMCs. Fig. 7(d) illustrates the ultimate compressive strength (σ_{cs}), 0.2% off-set yield strength ($\sigma_{0.2}$) and ultimate strain (ε) as a function of NDs concentration up to 0.5 wt%. For the sample of Ti/0.35%NDs, it has $\sigma_{0.2}$ value of 981 MPa that is 23.7% higher than that of pure Ti (793 MPa). With just 0.1% NDs, it shows 11.7% increases than that of the Ti (793 MPa). The ultimate compressive strength (σ_{bc}) of the nanocomposite increases from 0.1 to 0.25%, but decreases with increasing NDs content from 0.25% to 0.5%. This result can be attributed to the increments of NDs and nano-TiC phase. On the other hand, with the amount of NDs rising from 0.1 to 0.5%, ultimate strain (ε) of the nanocomposites decrease from 0.53 (53%) to 0.45 (45%). The NDs additives have improved the mechanical strength but the NDs and in-situ formed nano-TiC at expense of ductility. In general, the 0.35% NDs reinforced Ti matrix nanocomposite has the best integrated mechanical properties with remarkable increments in hardness and compressive strength with acceptable Young's modulus and less scarification of

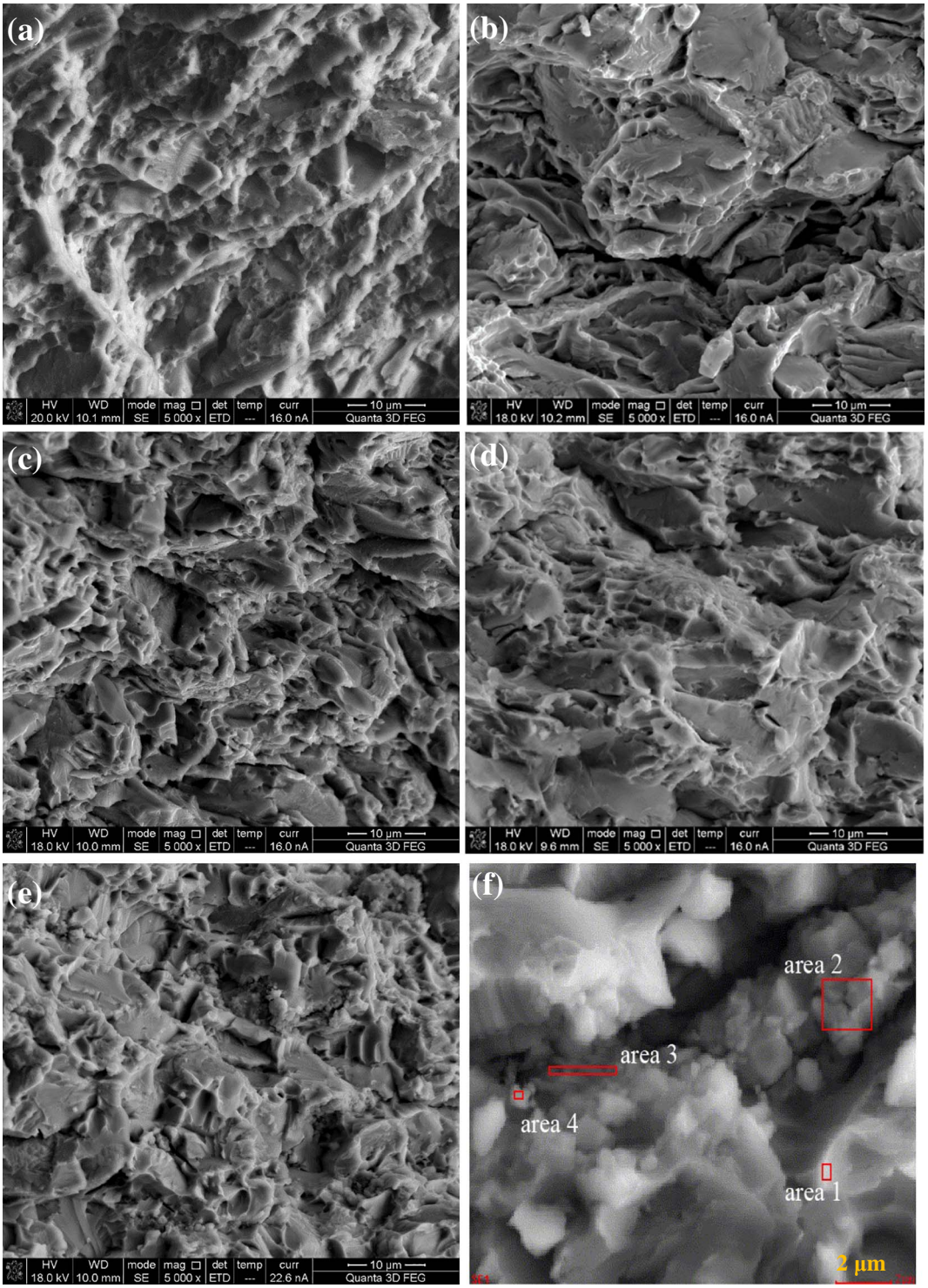

Fig. 8. SEM micrographs of the fractured surfaces of pure Ti (a), Ti/0.1% NDs (b), Ti/0.25% NDs (c), Ti/0.35% NDs (d) and Ti/0.5% NDs nanocomposites (e) with EDS inspection areas (f).

Table 2
EDS results of the marked areas in the fracture surfaces of the Ti/0.5 wt% NDs nanocomposites as shown in the Fig. 8(f).

Area	Ti (mass%)	C (mass%)	Ti (at%)	C (at%)
1	91.11	8.89	71.98	28.02
2	87.94	12.06	64.64	35.36
3	83.82	16.18	56.51	43.49
4	81.74	18.26	52.88	47.12

ductility. The Ti/0.1%NDs, Ti/0.25%NDs and Ti/0.35%NDs Ti MMCs all can be used with tailored mechanical properties by controlling the NDs concentration.

3.6. Strengthening mechanisms

The fracture surfaces of Ti/NDs nanocomposites are presented in Fig. 8. Fig. 8(a-d) shows the fracture surfaces of pure Ti, Ti/0.1%NDs, Ti/0.25%NDs, Ti/0.35%NDs nanocomposites, respectively. Obviously,

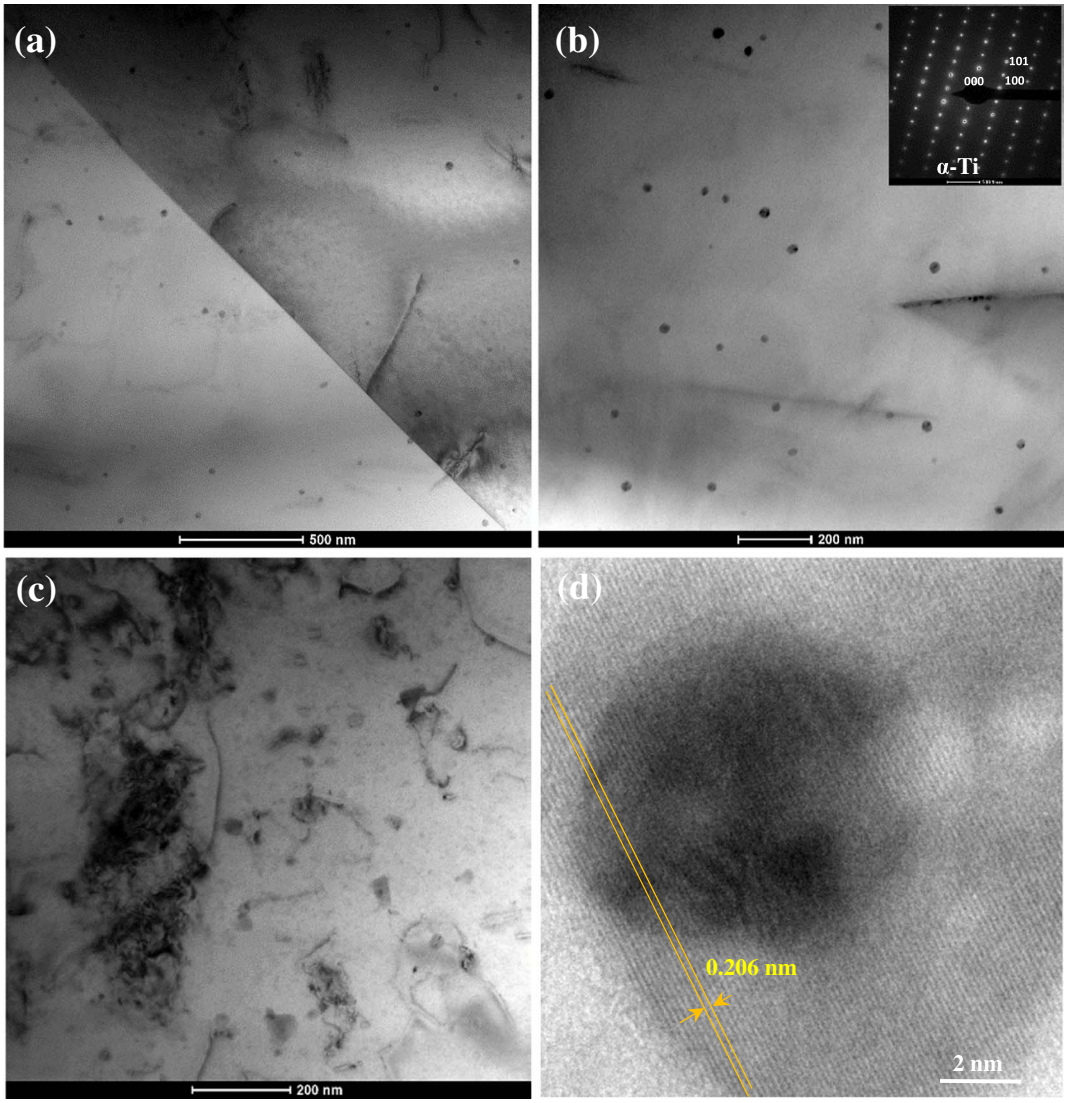

Fig. 9. TEM micrographs of the Ti/0.25% NDs nanocomposites with inserted selected area diffraction pattern (a-c) and HRTEM micrograph of the ND in the Ti matrix (d).

ductile dimples in the fracture surface can be observed. Fig. 8(e–f) shows the fracture surfaces of Ti/0.5%NDs nanocomposites. It clearly shows some crack steps with river pattern, indicating the nanocomposites have worse room temperature plasticity and ductility. Fig. 8(f) shows an FESEM image of intergranular fractured surface of the Ti/0.5%NDs, which was seriously damaged. The EDX analysis (Table 2) on the cracks (rectangular areas marked in Fig. 8f) provides evidences for the element distribution. As listed in Table 2, the carbon content shows a gradually increasing trend from area 1 to 4. It means that there are much more NDs or TiC in these sites. The Ti/0.5%NDs nanocomposites have much more nano-TiC phase generated on grain boundaries attributing to aggregation of NDs particles. The SEM fractured surfaces for the Ti/0.75–2.0 NDs composites show clearly the ND cluster gathering and the present of nano-TiC phase (Fig. S3). The occurrence of intergranular fracture at these sites results in overall grain pull-out and the particles situated in grain boundaries acting as crack initiation sites. Furthermore, the different coefficient of thermal expansion between Ti matrix and TiC lead to the weak bonding of the two parts. As a result, the mechanical properties (especially the ductility) of the Ti/0.5–2.0 NDs nanocomposites deteriorated.

Fig. 9 exhibits the TEM micrographs of the Ti/0.25%NDs nanocomposites. The TEM images (Fig. 9a, b) display the distribution and morphology of NDs in the Ti matrix. It is found that some spherical NDs with diameter of 5 nm are distributed uniformly throughout the matrix of the Ti/NDs nanocomposites. As can be seen in Fig. 9 (a, b), most of the ND particles of Ti/0.25% NDs nanocomposites were distributed relatively evenly in grains, rather than only gathering on grain boundaries. The SAD pattern confirmed the hcp structured α-Ti matrix. In addition, dislocation morphology in the Ti/0.25% NDs sample is found (Fig. 9c). There are some ND particles locating around the dislocations and causing a pinning effect, which is effective for improving the mechanical properties. In a high magnification image of the Ti/0.25% NDs nanocomposite (see Fig. 9d), the ND can be confirmed with d spacing of 0.206 nm corresponding to cubic diamond (111) plane. No interfacial reaction products (new phase such as TiC) and/or ND clusters cannot be observed in the grain boundary for Ti/0.25%NDs. The grain boundaries of the Ti/0.25%NDs are clear. Fig. 10 shows the TEM micrographs of the Ti/0.5% NDs nanocomposites with SAD patterns. In addition, the amounts of the NDs in Ti/0.5%NDs nanocomposites (Fig. 10a) increased significantly comparing to Ti/0.25%NDs nanocomposites (Fig. 9b). The SAD pattern on the Ti/0.5% NDs nanocomposites in Fig. 10(b) shows that these nanoparticles are cubic diamonds corresponding to the (111) and (220) planes of diamond in the matrix of α-Ti. A relative larger ND particle can be found in Fig. 10(c). It can be seen the different contrast between the ND and surrounding margin clearly. The SAD pattern confirms the presence of nano-TiC phase around the ND particle. The TEM and SAD results are consistent with the XRD results (Fig. 4) that the nano-TiC phase is formed in the

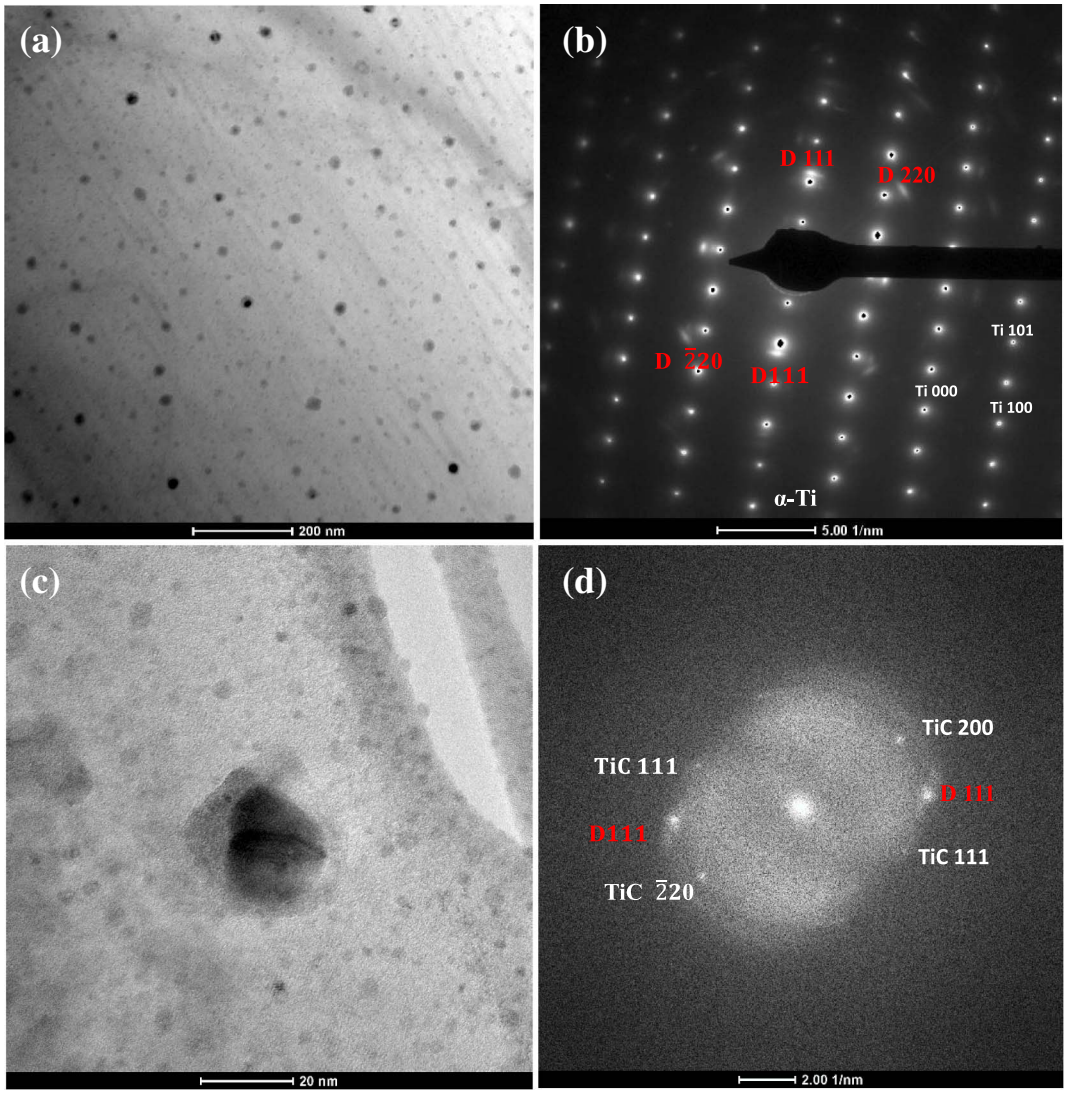

Fig. 10. TEM micrographs of the Ti/0.5% NDs nanocomposites (a, c) with selected area diffraction patterns (b, d).

Ti/0.5%NDs nanocomposites.

Based on the above results, the strengthening mechanisms of the Ti MMCs using NDs can be deduced. Firstly, these improvements in mechanical properties could be ascribed to the outstanding mechanical properties of ND, homogeneous dispersion of ND nanoclusters. Through microstructural study, it can be seen that the NDs are homogenously distributed in the matrix of Ti. When more amount of NDs are added, NDs particles are easily to aggregate on the grain boundaries and form nano-TiC phase. The NDs have many dangling bonds and large surface areas that allow them to bond with a variety of other materials. It is easy to generate nano-TiC phase due to the reaction between NDs and Ti. Secondly, dispersion strengthening using fine NDs and a certain amount of in-situ generated nano-TiC is regarded as the main strengthening mechanism. Small amount of in-situ formed nano-TiC particles could give rise to a pinning effect which is effective to strengthen the composite. However, the mechanical properties of Ti MMCs tended to deteriorate when the presence of much nano-TiC phases ($\geq$ 0.5 wt% NDs), particularly located on the grain boundaries, which acted as initiation site of crack. For MMCs containing fine particles, strengthening is often explained by the Orowan mechanism which caused by the resistance of closely spaced hard particles to the passing of dislocations [51–53]. Due to the presence of highly-dispersed non-shearable nanosized reinforcement particles (smaller than ~100 nm) in a metal matrix, the Orowan strengthening becomes more favorable in metal matrix nanocomposites. The Orowan mechanism can be explained by the following eq. [52],

$$\sigma_{Orowan} = \frac{2Gb}{2\pi(1-\nu)^{1/2}}\frac{1}{\lambda}ln(D/b) \quad (1)$$

where G is the shear modulus of matrix, b is the Burgers vector, ν is Poisson's ratio, D is the average diameter of nano-particles, λ is the inter-particle spacing and can be calculated as [53]:

$$\lambda = D\left(\frac{\pi}{6f_v} - \frac{2}{3}\right)^{1/2} \quad (2)$$

where f_v is the volume fraction of nanoparticles. Based on Eq. (1) and (2), it can be concluded that the mechanical properties of the MMCs can be improved by reducing the reinforcement particle size (D) and increasing fraction of the particles (f_v). Orowan strengthening using NDs and in-site formed nano-TiC plays an essential role in improving the mechanical properties of the Ti metal.

Secondly, solid solution strengthening of carbon atom is regarded as the second strengthening mechanism. In terms of the solution strengthening, the strengthening effect of C atom is up to the limit of solubility in the Ti matrix. Considering the solubility of only 0.05 wt% at room temperature, the carbon atoms dissolved into the crystal lattice of Ti when the content of NDs is 0.1 wt%, which can be verified in microstructural study. So the effect for attributing to solid solution

strengthening of carbon atom is almost the same for Ti/NDs composites when the content of NDs exceeds 0.1 wt%. Due to the limit of carbon solubility in Ti, solid solution strengthening effect has small differences among all the Ti/NDs composites. Finally, strengthening mechanisms mainly include Orowan strengthening and C atom solid solution strengthening. The results clarify that 0.35% NDs additive has the best effective strengthening effect as compared to other weight ratios of NDs. Coupled with the non-toxic property of NDs, the NDs reinforced Ti MMCs tailored with NDs from 0.1 to 0.35 wt% have much higher mechanical properties than that of pure Ti. They all have potentials for biomedical applications, especially for hard-tissue repair applications as bone substitutes and dental implants.

4. Conclusions

The Ti/ND nanocomposites were fabricated by the SPS method. Dense Ti/ND nanocomposites were fabricated by SPS at 900 °C for 10 min under pressure of 60 MPa in vacuum. The relative densities of the Ti/NDs nanocomposites decreased with an increase of the NDs concentration. Pure α-Ti phase was found in the XRD patterns of the Ti MMCs with NDs from 0.1 to 0.35%. Few amount of nano-TiC phase was observed in the XRD pattern of the Ti/0.5–2.0%NDs. The metallographic images exhibited that the amounts of voids increased with the fraction of NDs increases. The SEM with EDS results indicated that the distributions of C elements are both in the grain boundaries and inside of the grains. The NDs are easier to concentrate in the grain boundaries rather than in the grains.

The nanoindentation hardness and Young's modulus of the Ti MMCs are significantly increased with increasing of the NDs concentration. The Ti/NDs nanocomposites all exhibit much higher yield strength (0.2% off-set) when compared to that of pure Ti. The ultimate strain of the nanocomposites decreases from 53% to 34% with increasing of NDs from 0.1 to 2.0%. The Ti/0.35% NDs have the best integrated mechanical properties with remarkable increments in hardness (52.3%) and compressive yield strength (23.7%) with acceptable Young's modulus (129 GPa) and less scarification of ductility (49%). The outstanding mechanical properties of NDs, homogeneous dispersion of ND nanoclusters, Orowan strengthening with NDs and in-situ formed nano-TiC play the essential role in improving the mechanical properties of the Ti. Carbon atom solid solution strengthening is regarded as the second strengthening mechanism. The NDs are effective nanostructured reinforcements for the Ti MMCs and the Ti/NDs nanocomposites have potential for biomedical applications.

Acknowledgment

The authors gratefully acknowledge the financial supports from Natural Science Foundation of Jiangsu Province (No. BK20161419), Opening Project of State Key Laboratory of High Performance Ceramics and Superfine Microstructure at SICCAS (No·SKL201603SIC), Scientific Research Foundation for the Returned Overseas Chinese Scholars at State Education Ministry (No. 2015-1098), State Key Laboratory for Powder Metallurgy (No. 201403) at Central South University, Jiangsu Key Laboratory for Advanced Metallic Materials (No. BM2007204) at Southeast University, and the Fundamental Research Funds for the Central Universities (No. 2242017K40183).

Appendix A. Supplementary data

Supplementary data to this article can be found online at http://dx.doi.org/10.1016/j.matdes.2017.06.015.

References

[1] C. Qiu, A. Fones, H.G.C. Hamilton, N.J.E. Adkins, M.M. Attallah, A new approach to develop palladium-modified Ti-based alloys for biomedical applications, Mater. Des. 109 (2016) 98–111.
[2] M. Geetha, A.K. Singh, R. Asokamani, A.K. Gogia, Ti based biomaterials, the ultimate choice for orthopaedic implants - a review, Prog. Mater. Sci. 54 (2009) 397–425.
[3] C. Aparicio, F.J. Gil, C. Fonseca, M. Barbosa, J.A. Planell, Corrosion behaviour of commercially pure titanium shot blasted with different materials and sizes of shot particles for dental implant applications, Biomaterials 24 (2003) 263–273.
[4] H.J. Rack, J.I. Qazi, Titanium alloys for biomedical applications, Mater. Sci. Eng. C 26 (2006) 1269–1277.
[5] I. Dion, C. Baquey, J.R. Monties, P. Havlik, Haemocompatibility of Ti6A14V alloy, Biomaterials 14 (1993) 122–126.
[6] D. Kuroda, H. Kawasaki, S. Hiromoto, T. Hanawa, Development of new Ti/Fe-Ta and Ti/Fe-Ta-Zr system alloys for biomedical applications, Mater. Trans. 46 (2005) 1532–1539.
[7] T. Namura, Y. Fukui, H. Hosoda, K. Wakashima, S. Miyazaki, Mechanical properties of Ti/Nb biomedical shape memory alloys containing Ge or Ga, Mater. Sci. Eng. C 25 (2005) 426–432.
[8] W.F. Ho, W.K. Chen, S.C. Wu, H.C. Hsu, Structure, mechanical properties, and grindability of dental Ti–Zr alloys, J. Mater. Sci. Mater. Med. 19 (2008) 3179–3186.
[9] L.Z. Ying, M. Niinomi, T. Akahori, H. Fukui, H. Toda, Corrosion resistance and biocompatibility of Ti/Ta alloys for biomedical applications, Mater. Sci. Eng. A 398 (2005) 28–36.
[10] D.J. Lin, C. Chuang, J.H. Chern Lin, J.W. Lee, C.P. Ju, H.S. Yin, Bone formation at the surface of low modulus Ti–7.5Mo implants in rabbit femur, Biomaterials 28 (2007) 2582–2589.
[11] D. Bogdanski, M. Köller, D. Müller, G. Muhr, M. Bram, H.P. Buchkremer, D. Stöver, J. Choi, E. Matthias, Easy assessment of the biocompatibility of Ni–Ti alloys by in vitro cell culture experiments on a functionally graded Ni–NiTi–Ti material, Biomaterials 23 (2002) 4549–4555.
[12] K.T. Oh, D.K. Kang, G.S. Choi, K.N. Kim, Cytocompatibility and electrochemical properties of Ti–Au alloys for biomedical applications, J. Biomed. Mater. Res. 83B (2007) 320–326.
[13] D. Handtrack, F. Despang, C. Sauer, B. Kieback, N. Reinfried, Y. Grin, Fabrication of ultra-fine grained and dispersion-strengthened titanium materials by spark plasma sintering, Mater. Sci. Eng. A 437 (2006) 423–429.
[14] F. Zhang, A. Weidmann, J.B. Nebe, U. Beck, E. Burkel, Preparation, microstructures, mechanical properties and cytocompatibility of TiMn alloys for biomedical applications, J. Biomed. Mater. Res. B Appl. Biomater. 94B (2010) 406–413.
[15] Y. Okazaki, E. Gotoh, Comparison of metal release from various metallic biomaterials in vitro, Biomaterials 26 (2005) 11–21.
[16] T. Hanawa, Metal ion release from metal implants, Mater. Sci. Eng. C 24 (2004) 745–752.
[17] J.G. Park, D.H. Keum, Y.H. Lee, Strengthening mechanisms in carbon nanotube-reinforced aluminum composites, Carbon 95 (2015) 690–698.
[18] A.O. Adegbenjo, P.A. Olubambi, J.H. Potgieter, M.B. Shongwe, M. Ramakokovhu, Spark plasma sintering of graphitized multi-walled carbon nanotube reinforced Ti6Al4V, Mater. Des. 128 (2017) 119–129.
[19] X.Y. Liu, F.C. Wang, W.Q. Wang, H.A. Wu, Interfacial strengthening and self-healing effect in graphene-copper nanolayered composites under shear deformation, Carbon 107 (2016) 680–688.
[20] X. Feng, J.H. Sui, Y. Feng, W. Cai, Preparation and elevated temperature compressive properties of multiwalled carbon nanotube reinforced Ti composites, Mater. Sci. Eng. A 527 (2010) 1586–1589.
[21] K. Kondoh, T. Threrujirapapong, J. Umeda, B. Fugetsu, High-temperature properties of extruded titanium composites fabricated from carbon nanotubes coated titanium powder by spark plasma sintering and hot extrusion, Compos. Sci. Technol. 72 (2012) 1291–1297.
[22] K. Kondoh, T. Threrujirapapong, H. Imai, J. Umeda, B. Fugetsu, Characteristics of powder metallurgy pure titanium matrix composite reinforced with multi-wall carbon nanotubes, Compos. Sci. Technol. 69 (2009) 1077–1081.
[23] F.C. Wang, Z.H. Zhang, Y.J. Sun, Y. Liu, Z.Y. Hu, et al., Rapid and low temperature spark plasma sintering synthesis of novel carbon nanotube reinforced titanium matrix composites, Carbon 95 (2015) 396–407.
[24] N. Lewinski, V. Colvin, R. Drezek, Cytotoxicity of nanoparticles, Small 4 (2008) 26–49.
[25] A. Shvedova, V. Castranova, E. Kisin, D. Schwegler-Berry, A. Murray, V. Gandelsman, et al., Exposure to carbon nanotube material: assessment of nanotube cytotoxicity using human keratinocyte cells, J. Toxic. Environ. Health A 66 (2003) 1909–1926.
[26] V.C. Sanchez, A. Jachak, R.H. Hurt, A.B. Kane, Biological interactions of graphene-family nanomaterials: an interdisciplinary review, Chem. Res. Toxicol. 25 (2012) 15–34.
[27] Z. Singh, Applications and toxicity of graphene family nanomaterials and their composites, Nanotechnol. Sci. Appl. 9 (2016) 15–28.
[28] L. Ou, B. Song, H. Liang, J. Liu, X. Feng, B. Deng, et al., Toxicity of graphene-family nanoparticles: a general review of the origins and mechanisms, Part. Fibre Toxicol. 13 (2016) 1–24.
[29] V.N. Mochalin, O. Shenderova, D. Ho, Y. Gogotsi, The properties and applications of nanodiamonds, Nat. Nanotechnol. 7 (2012) 11–23.
[30] A.M. Schrand, L. Dai, J.J. Schlager, S.M. Hussain, E. Osawa, Differential biocompatibility of carbon nanotubes and nanodiamonds, Diam. Relat. Mater. 16 (2007) 2118–2123.
[31] S.G. Lichter, M.C. Escudié, A.D. Stacey, K. Ganesan, K. Fox, A. Ahnood, et al., Hermetic diamond capsules for biomedical implants enabled by gold active braze alloys, Biomaterials 53 (2015) 464–474.
[32] S.T. Bhattacherjee, H. Niakan, Q.Q. Yang, Y.F. Hu, J. Dynes, Enhancement of

adhesion and corrosion resistance of diamond-like carbon thin films on Ti-6Al-4V alloy by nitrogen doping and incorporation of nanodiamond particles, Surf. Coat. Technol. 284 (2015) 153–158.
[33] H.C. Chang, Development and use of fluorescent nanodiamonds as cellular markers, in: D. Ho (Ed.), Nanodiamonds: Applications in Biology and Nanoscale Medicine, Springer, New York, 2010, pp. 127–150.
[34] H. Huang, E. Pierstorff, K. Liu, E. Ōsawa, D. Ho, Nanodiamond-mediated delivery of therapeutics via particle and thin film architectures, in: D. Ho (Ed.), Nanodiamonds: Applications in Biology and Nanoscale Medicine, Springer, New York, 2010, pp. 151–174.
[35] R. Lam, M. Chen, H. Huang, E. Ōsawa, D. Ho, Polymeric encapsulation of nanodiamond-chemotherapeutic complexes for localized cancer treatment, in: D. Ho (Ed.), Nanodiamonds: Applications in Biology and Nanoscale Medicine, Springer, New York, 2010, pp. 249–284.
[36] Y.Q. Zhao, K.T. Lau, J.K. Kim, C.L. Xu, D.D. Zhao, H.L. Li, Nanodiamond/poly (lactic acid) nanocomposites: Effect of nanodiamond on structure and properties of poly (lactic acid), Compos. Part B 41 (2010) 646–653.
[37] K. Hanada, K. Yamamato, T. Taguchi, E. Osawa, M. Inakuma, V. Livramento, et al., Further studies on copper nanocomposite with dispersed single-digit nanodiamond particles, Diam. Relat. Mater. 16 (2007) 2054–2057.
[38] H. Kaftelen, M. Öveçoğlu, Microstructural characterization and wear properties of ultra-dispersed nanodiamond (UDD) reinforced Al matrix composites fabricated by ball-milling and sintering, J. Compos. Mater. 46 (2012) 1521–1534.
[39] D.J. Woo, F.C. Heer, L.N. Brewer, J.P. Hooper, S. Osswald, Synthesis of nanodiamond-reinforced aluminum metal matrix composites using cold-spray deposition, Carbon 86 (2015) 15–25.
[40] A.P. Vladimir, E.V. Shelekhov, E.V. Vershinina, Influence of reinforcing non-agglomerated nanodiamond particles on metal matrix nanocomposite structure stability in the course of heating, Eur. J. Inorg. Chem. 10 (2016) 2122–2124.
[41] I.M. Melendez, E. Neubauer, P. Angerer, H. Danninger, J.M. Torralba, Influence of nano-reinforcements on the mechanical properties and microstructure of titanium matrix composites, Compos. Sci. Technol. 71 (2011) 1154–1162.
[42] A. Nieto, D. Lahiri, A. Agarwal, Synthesis and properties of bulk grapheme nanoplatelets consolidated by spark plasma sintering, Carbon 50 (2012) 4068–4077.
[43] F. Zhang, M. Reich, O. Kessler, E. Burkel, Potential of rapid cooling spark plasma sintering for metallic materials, Mater. Today 16 (2013) 192–195.
[44] F. Saba, F. Zhang, S.A. Sajjadi, M. Haddad-Sabzevar, P. Li, Pulsed current field assisted surface modification of carbon nanotubes with nanocrystalline titanium carbide, Carbon 101 (2016) 261–271.
[45] A. Ibrahim, F. Zhang, E. Otterstein, E. Burkel, Processing of porous Ti and Ti5Mn foams by spark plasma sintering, Mater. Des. 32 (2011) 146–153.
[46] M. Elahiniaa, N.S. Moghaddama, M.T. Andania, A. Amerinatanzia, B.A. Bimberc, R.F. Hamiltonc, Fabrication of NiTi through additive manufacturing: a review, Prog. Mater. Sci. 83 (2016) 630–663.
[47] V. Popov, D. Többens, A. Prosviryakov, Identification of non-agglomerated nanodiamonds inside metal matrix composites by synchrotron radiation, Phys. Status Solidi A 211 (2014) 2353–2358.
[48] S.F. Li, B. Sun, I. Hisashi, M. Takanori, K. Katsuyoshi, Powder metallurgy titanium metal matrix composites reinforced with carbon nanotubes and graphite, Compos. A: Appl. Sci. Manuf. 48 (2013) 57–66.
[49] M.I. De Barros, D. Rats, L. Vandenbulcke, G. Farges, Influence of internal diffusion barriers on carbon diffusion in pure titanium and Ti-6Al-4V during diamond deposition, Diam. Relat. Mater. 8 (1999) 1022–1032.
[50] B.K.C. Ganesh, W. Sha, N. Ramanaiah, A. Krishnaiah, Effect of shotpeening on sliding wear and tensile behavior of titanium implant alloys, Mater. Des. 56 (2014) 480–486.
[51] H. Wen, T.D. Topping, D. Isheim, D.N. Seidman, E.J. Lavernia, Strengthening mechanisms in a high-strength bulk nanostructured Cu-Zn-Al alloy processed via cryomilling and spark plasma sintering, Acta Mater. 61 (2013) 2769–2782.
[52] Q. Sylvain, M. Ghiath, D. Benotit, Orowan strengthening and forest hardening superposion examined by dislocation dynamics simulations, Acta Mater. 58 (2010) 5586–5595.
[53] X.C. Tong, A.K. Ghosh, Fabrication of in situ TiC reinforced aluminum matrix composites, J. Mater. Sci. 36 (2001) 4059–4069.